CrossMark

ORIGINAL ARTICLE

# Numerical modeling and experiment of counter-gravity casting for titanium alloys

Shouyin Zhang[1,2] · Jinshan Li[1] · Hongchao Kou[1] · Jieren Yang[1] · Guang Yang[1] · Jun Wang[1]

**Abstract** The filling capacity and solidification behavior during counter-gravity casting of the titanium alloy Ti-6Al-4V were investigated. ProCAST code was used to optimize filling technology and predict defects through casting simulation. Cast parts with highly accurate dimensions were acquired. The filling capacity and positions of shrinkage porosity were in good agreement with those predicted via simulation. Tensile test results showed that the cast parts of Ti-6Al-4V produced via counter-gravity casting exhibit good balance between strength and ductility, which are comparable to tensile properties of cast Ti-6Al-4V produced in gravity casting subjected to hot isostatic pressing + annealing status.

**Keywords** Counter-gravity casting · Ti-6Al-4V · Numerical modeling · Tensile test

## 1 Introduction

Titanium and its alloys have been used in advanced aerospace structural applications because of their excellent combination of ductility, fracture toughness, and high strength-to-weight ratio [1, 2]. Investment casting is applied to produce components with excellent surface finish, dimensional accuracy, and complex shapes [3]. High-performance titanium alloy castings are mainly produced via investment casting technique [4]. High-temperature isostatic pressing (HIP) was used to result in substantial improvement in mechanical properties of cast titanium alloys by a significant reduction in porosity. Numerical simulation have also become increasingly sophisticated to guarantee the precision and increase the yield rate of titanium alloys. Besides, some casting techniques, such as centrifugal casting and counter-gravity casting, were used to improve the fluidity of titanium alloys and minimize the casting defects, aimed to obtain high-performance titanium alloy castings.

Centrifugal casting can be used to produce good cast parts by increasing the fluidity of titanium alloy liquid as a consequence of centrifugal force. Li et al. [5] fabricated titanium alloys via centrifugal casting and found that the forming ability of thin-walled titanium alloy increases as rotational velocity increases. For counter-gravity casting, pressure can be applied to the melt by introducing air or inert gas when a mold is placed on a crucible with melt liquid and is attached to a riser tube. As such, the melt in the crucible is forced to travel upward and fill the mold. Given that the metal liquid is driven by pressure, the filling capacity of counter-gravity casting is greater than that of gravity casting, especially for thin-walled cast parts. Thus, it can be speculated that the combination of counter-gravity casting and investment casting may be suitable to manufacture thin-walled complex cast parts with high filling capacity and dimension accuracy. Nevertheless, technical problems, such as melt and filling, should be resolved because of high melting point and strong chemical affinity of titanium and its alloys. Studies on counter-gravity casting of titanium alloys are limited. For instance, Daido Castings Co., Ltd., invented a new counter-gravity casting technique called Levicast, which exhibits three advantages, namely, contamination-free melt, thin wall casting, and high

✉ Hongchao Kou
hchkou@nwpu.edu.cn

[1] State Key Laboratory of Solidification Processing, Northwestern Polytechnical University, 127 West Youyi Road, Xi'an 710072, China

[2] School of Aeronautic Manufacturing Engineering, Nanchang Hangkong University, Nanchang 330063, China

productivity [6]. Investment and suction casting has also been applied to fabricate γ-TiAl-based alloys in automotive exhaust valves [7].

The present work aims to investigate the process of counter-gravity casting on Ti-6Al-4V, a widely used titanium alloy. Cast parts in the form of sheets and bars with different sizes were designed. CAE package ProCAST based on a finite element method (FEM) was used to predict the filling and solidification behavior of counter-gravity casting. Counter-gravity casting was performed using the parameters optimized through numerical simulations. Defects, such as shrinkage porosity, were analyzed via radiographic testing. The mechanical properties of bars were also evaluated via tensile tests.

## 2 Materials and methods

### 2.1 Experiment

#### 2.1.1 Cast part design and ceramic shell manufacturing

Cast part in the form of sheets and bars with different sizes were designed (Fig. 1a). The specific dimensions are listed as follows: bars ($\Phi 10 \times 180$, $\Phi 15 \times 180$, $\Phi 20 \times 180$ mm) and sheets (2, 3, 6, 9 mm)$\times 50 \times 180$ mm.

The process involved in investment casting includes wax pattern manufacturing, ceramic shell building, dewaxing, pouring, and finishing. Wax patterns of bars and sheets with different dimensions were injected separately and assembled using runners, risers, and sprue.

Due to the strong affinity of Ti to elements such as O, N, or C and its high melting point of 1668 °C leading to reactions with the investment surface [8], the primary coating is prepared using yttrium oxide power and zirconium acetate. The pattern was continuously stuccoed with coarse zircon sand till the thickness of the ceramic shell reaches approximately 6 mm. The molds are dewaxed via autoclave dewaxing. The obtained ceramic shell materials are fired for 12 h to remove moisture, to burn off residual pattern material, and to sinter the ceramic. The ceramic shell after dewaxing is shown in Fig. 1b.
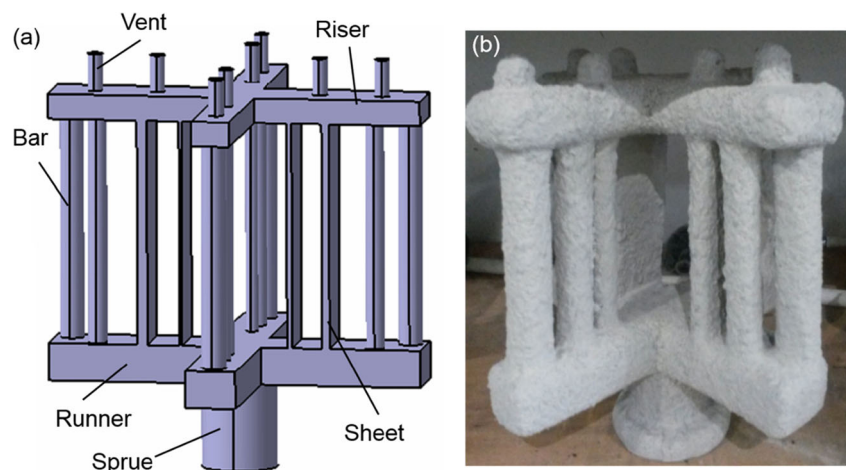
#### 2.1.2 Counter-gravity casting process

The outline of the counter-gravity casting device used in this study is shown in Fig. 2. The water-cooled copper crucible is placed on a lifting mechanism in the bottom chamber, whereas the sand box with ceramic shell is placed on the top chamber. The two chambers are connected by a riser tube, which is designed for the rising of the melt.

Both chambers are sealed, vacuumed, and backfilled with Ar gas to approximately 200 Pa to minimize titanium alloy oxidation. The ingot in the crucible is heated and melted using an inductor coil. The water-cooled copper crucible contained vertical slits around it for electrical insulation, and eddy current is generated in the molten metal [6]. With the rise tuber immersed in the melt, the top and bottom chambers become separated when the cold crucible rises with the lifter. High-pressure Ar gas is immediately introduced to the bottom chamber. Due to the effect of pressure on the liquid surface, the melt rises in the riser tuber, followed by the ceramic shell. The pressure between the bottom and top chambers can be maintained until the cast part is completely solidified.

Radiographic testing was performed to analyze defects such as shrinkage porosity. Figure 3 presents the schematic method on how grain size was measured. The tensile properties of the alloy bars with different diameters ($\Phi 10$, $\Phi 15$, and $\Phi 20$ mm) were evaluated at room temperature. The tensile test of each diameter was repeated twice, and the average of the two tensile results were obtained to confirm the validity of the

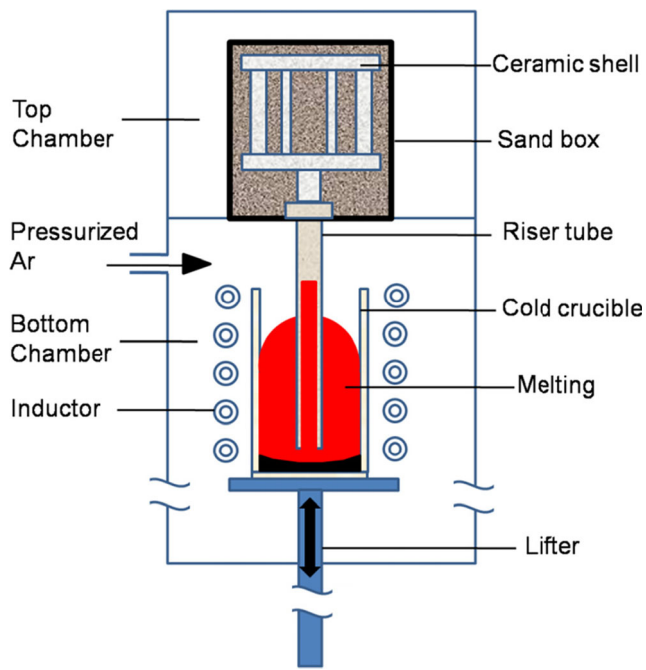Fig. 1 **a** Geometry. **b** Ceramic shell after dewaxing

Fig. 2 Schematic of counter-gravity casting

tensile test results. The error range was also included in the experimental data.

## 2.2 Mathematical model

ProCAST (ESI Group), a casting simulation package, was used to simulate casting by numerically solving Navier–Stokes (fluid flow) and Fourier (heat transfer) equations. Radiation heat transfer was simulated between the external surface of the mold and the chamber wall by using an effective heat transfer coefficient, which can be written as follows [9]:

$$h = \sigma\varepsilon\left(T_1^2 + T_2^2\right)(T_1 + T_2), \tag{1}$$

where $\varepsilon$ is the emissivity of the molten metal and heated mold material in both forms with heat transferred through radiation, $\sigma$ is the Stefan–Boltzmann constant ($\sigma=5.670\times$
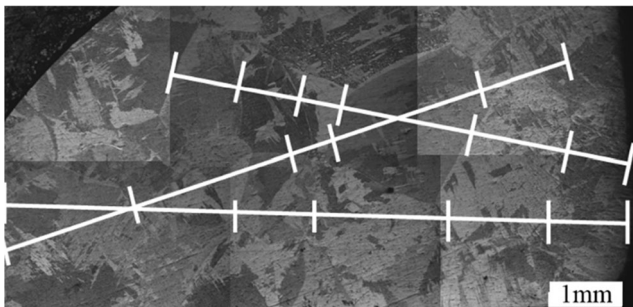


Fig. 3 Schematic showing how grain size was measured. The macroscopic image is composed of six individual micrographs

$10^{-8}$ W m$^{-2}$ K$^{-4}$), and $T_1/T_2$ are temperatures of the two bodies involved in heat transfer.

Shrinkage porosity was quantitatively predicted using a built-in "feeding criterion" function. With the obtained temperature field, Niyama criterion [10], which is the most widely used criterion function of metal casting [11], is utilized in this study to predict the feeding-related shrinkage porosity. The Niyama criterion is a local thermal parameter defined as follows:

$$Ny = \frac{G}{\sqrt{T}}, \tag{2}$$

where $G$ is the temperature gradient and $T$ is the cooling rate; these parameters are evaluated at a specified temperature near the end of solidification.

## 3 Results and discussions

### 3.1 Mold filling

#### 3.1.1 Mold filling in simulation

The required minimum pressure applied to the surface of the melt in the crucible can be calculated by applying Pascal's principle:
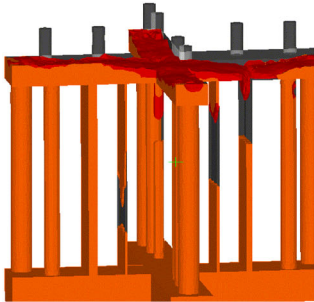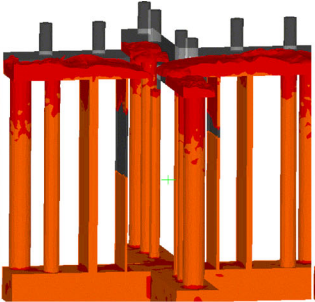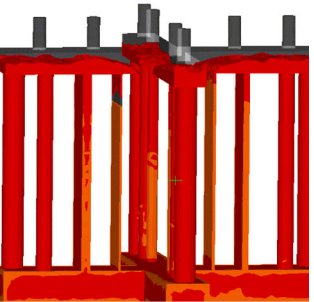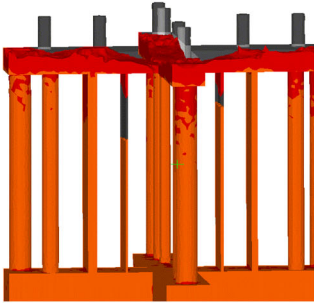
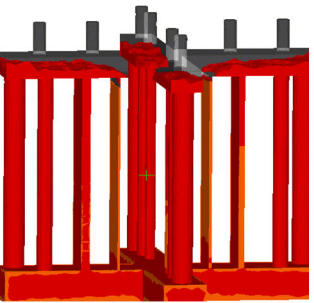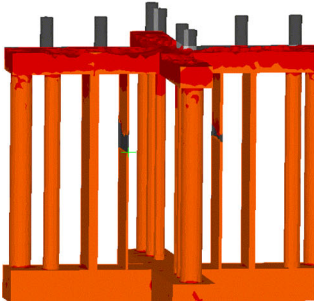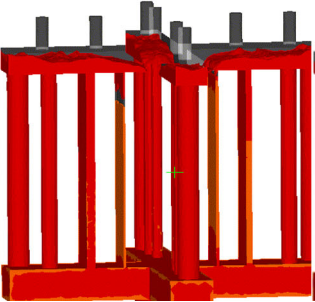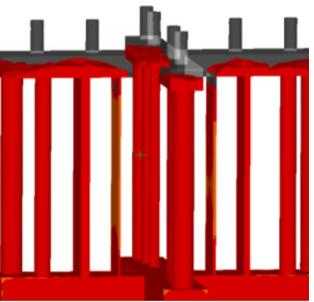$$\Delta P = \rho g \Delta H, \tag{3}$$
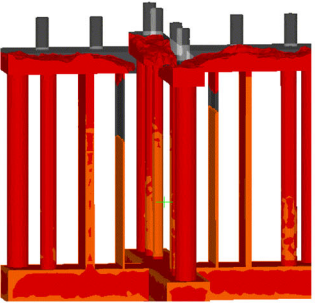
where $\Delta P$ is the hydrostatic pressure, in pascals; $\rho$ is the density of the metal liquid, in kilograms per cubic meter; $g$ is the acceleration caused by gravity, in meter per second squared; and $\Delta H$ is the height difference between the top of the mold and the surface of the metal liquid in the crucible after the mold is filled, in meters.

$\rho$ of the Ti-6Al-4V metal liquid is approximately 4.5× $10^3$ kg m$^{-3}$, $g$ is 9.81 m s$^{-2}$, and $\Delta H$ in the experiment is 1 m. $\Delta P$ is approximately 44 kPa. Considering pressure losses and energy consumption, we set the filling pressure at 60 kPa.

After the filling pressure was set, the major factors affecting the filling process include pressurization rate, pouring temperature, and mold temperature. Initial simulations were conducted to investigate the filling process with different parameters during counter-gravity casting. The liquidus and solidus temperature are 1660 and 1605 °C, respectively. The heat transfer coefficient between casting and ceramic shell is 500 W m$^{-2}$ K$^{-1}$. The results with different boundary conditions are shown in Table 1.

Defects likely appear in sheets with dimensions of 2 and 3 mm, but the effect is more severe in the former than in the latter. The melt will merge at the top of the sheets,

**Table 1** Simulation results of the filling process with different parameters

| Pressurization rate | Pouring Temp 1710 °C Mold Temp 300 °C | Pouring Temp 1760 °C Mold Temp 300 °C | Pouring Temp 1760 °C Mold Temp 650 °C |
|---|---|---|---|
| 6 kPa s$^{-1}$ | | | |
| 9 kPa s$^{-1}$ | | | |
| 15 kPa s$^{-1}$ | | | |



resulting in defects, such as cold shut or slag inclusion. As pressurization rate increased, filling capacity improved. The filling distance of the 2-mm sheet increased as pouring and mold temperatures increased. The results at pressurization rates of 9 and 15 kPa s$^{-1}$, pouring temperature of 1760 °C, and mold temperature of 650 °C were acceptable, although defects might appear at the top of the 2-mm sheet. A pressurization rate of 9 kPa s$^{-1}$, pouring temperature of 1760 °C, and mold temperature of 650 °C were selected as optimum casting parameters when the pressurization rate of the counter-gravity casting equipment was considered.

With the optimized casting parameters, the filling process of the simulation is shown in Fig. 4. The corresponding temperature color coding is also shown on the right. It can be observed that the filling time was 5.6 s when pressurization rate was 9 kPa s$^{-1}$. The riser tube and the runner were filled in sequence. Then, the melt started to enter the bars and sheets. In Fig. 4d, the bars and sheets were completely filled. No turbulence was observed on the melt surface during filling.

When zoomed in Fig. 4d, close examination revealed that the melt backfill appeared at the top of the 2-mm sheet. Meanwhile, the temperature at the top of 2-mm sheet was less than the liquid line, resulting in cold shut.

**Fig. 4** Mold filling sequence of numerical simulation at different times: *a* 2.7 s; *b* 4.2 s; *c* 4.7 s; *d* 5.2 s; *e* 5.6 s
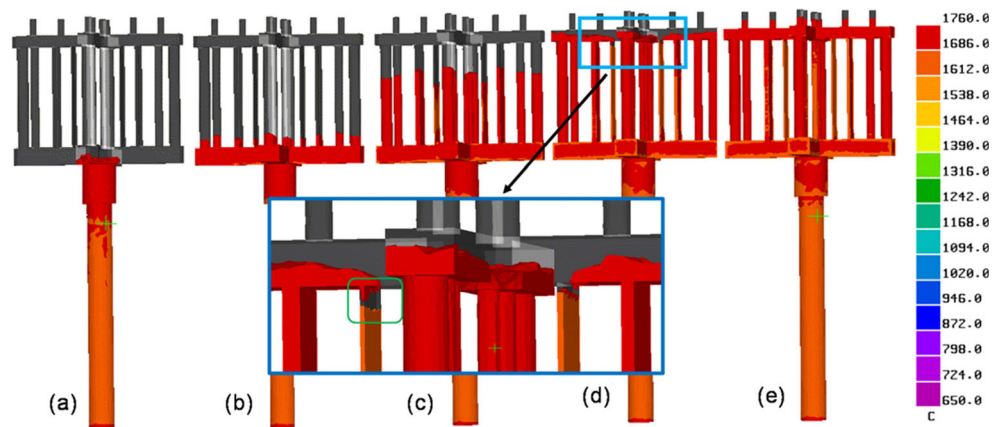
### 3.1.2 Filling capacity

The filling process of counter-gravity casting can be separated into two stages. In the first stage, pressure is exerted to force the melt to rise in the riser tube to the gate of the mold. In the second stage, pressure is increased to push the melt into the ceramic shell. The velocity of the melt should be controlled to ensure that the melt completely fills the ceramic shell without any splash.

Fluid flow can be considered as laminar in a tube when Reynolds number, Re, is <2100, and turbulent flow occurs when Re>4000 [12]. Reynold's number can be expressed as follows:

$$\mathrm{Re} = \frac{\rho v D_{\mathrm{H}}}{\mu}, \tag{4}$$

where $v$ is the velocity of the melt (m s$^{-1}$), $\rho$ is the density (kg m$^{-3}$), $D_{\mathrm{H}}$ is the hydraulic diameter of the pipe, and $\mu$ is the viscosity of the melt (N s m$^{-2}$).

For the Ti-6Al-4V melt, $\rho$ is $4.5 \times 10^3$ kg m$^{-3}$ and $\mu$ is $5 \times 10^{-3}$ N s m$^{-2}$. Based on Eq. 4, critical Re of 2100 and 4000 correspond to 0.05 and 0.09 m/s, respectively. With such a low filling velocity, the temperature of the melt rapidly decreases, especially for high-temperature alloys. Thus, the integrity of casting cannot be guaranteed. This phenomenon might occur because the melt vertically fills the riser tube, and the critical Re corresponds to fluids that horizontally flow in a pipe [13]. In addition, the filling process of casting is a transient flow, not a steady process. Therefore, the Re principle might not be applicable in the filling process of counter-gravity casting. Conversely, a high velocity causes turbulence, gas entrapment, or mold damage. An optimum velocity at which a liquid metal enters a mold should be determined. This critical velocity is close to 0.5 m s$^{-1}$ for almost all liquid metals according to Campbell [14] and Itamura et al. [15]. In this scope, the melt rises to an appropriate height that can be supported by surface tension around the periphery of the spreading drop. Otherwise, the
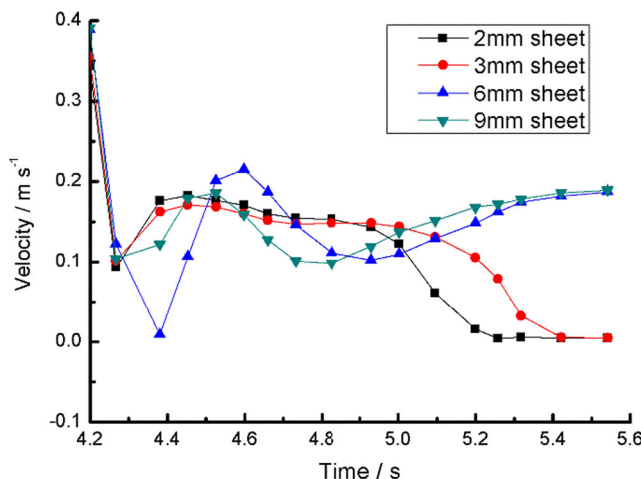
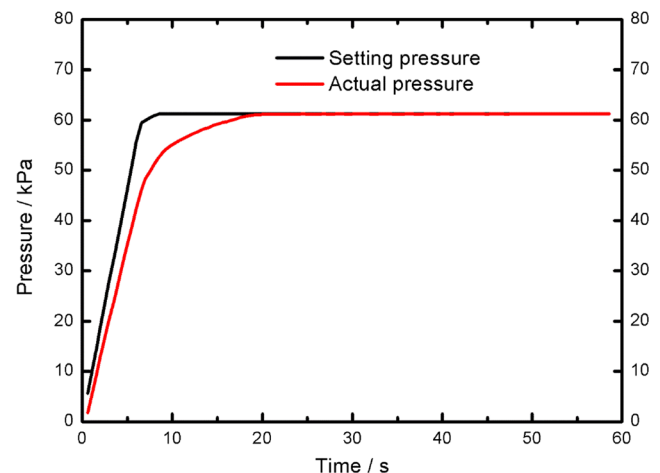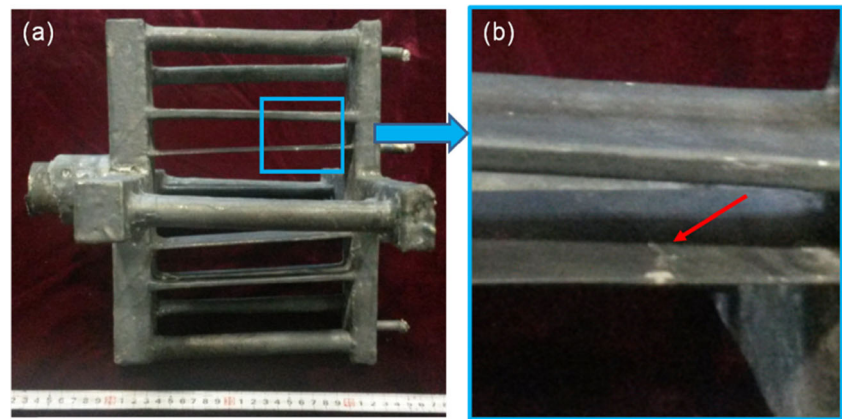**Fig. 5** Velocity of melt in the sheets

**Fig. 6** Setting and actual pressure in the casting process

Fig. 7  **a** Cast part. **b** Cold shut defect



instability in the free surface of the liquid metal might lead to the defects, which will become the sources of the cracks or hot tears [16].

The riser tube with a length of 0.6 m was filled at 2.7 s, as depicted in the simulation results in Fig. 4. The average melt velocity in riser tube was 0.22 m s$^{-1}$. According to the critical velocity principle, the melt will rise in the riser tube steadily without causing any entrapment defects. Figure 5 shows the velocity of the melt at the bottom of the sheets, which was placed approximately 5 mm away from the runner. The highest velocity was observed in the beginning of filling process. The velocity was below 0.4 m s$^{-1}$, which is within the slope of the critical velocity. Ar gas in the ceramic shell is pushed

ahead of the metal liquid, and no surface entrainment occurs.

The fluid velocity of 2- and 3-mm sheets decreased at 5.0 s as shown in Fig. 5. The fluid velocity of 2-mm sheet decreased to 0 m s$^{-1}$ after 5.2 s; this result indicated that the melt ceases to fill and solidify because temperature decreases. The same phenomenon was observed in 3-mm sheet at 5.4 s. However, the flow channels in 6- and 9-mm sheets did not close until the end of the filling process. The main disadvantage of titanium and its alloys is their low castability because of low fluidity and high reactivity [4]. The experimental results showed that the application of counter-gravity casting can overcome the relatively low fluidity of titanium alloys, especially for thin-walled castings.

Fig. 8  Contours of temperature in solidification process. **a** 26 s. **b** 120 s. **c** 250 s. **d** 400 s
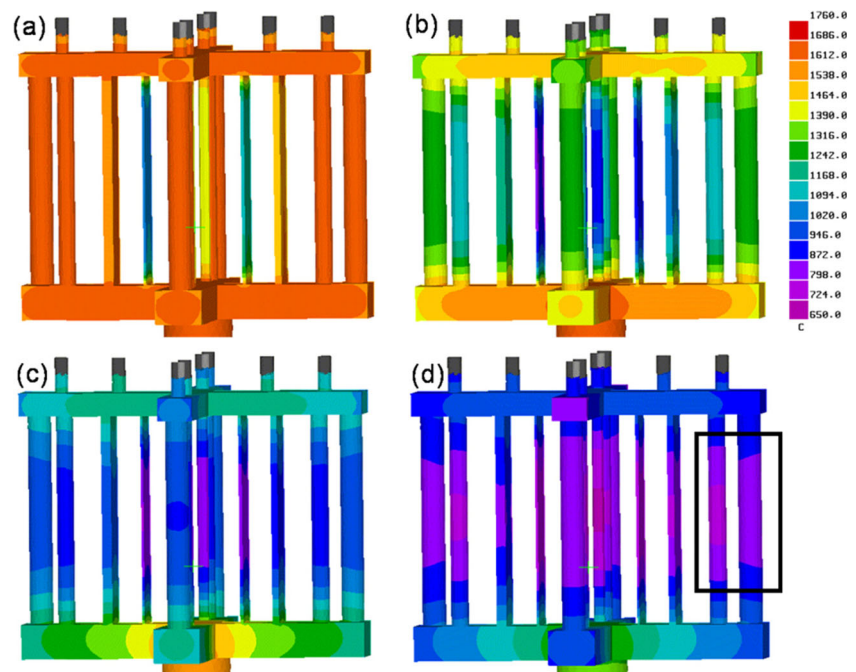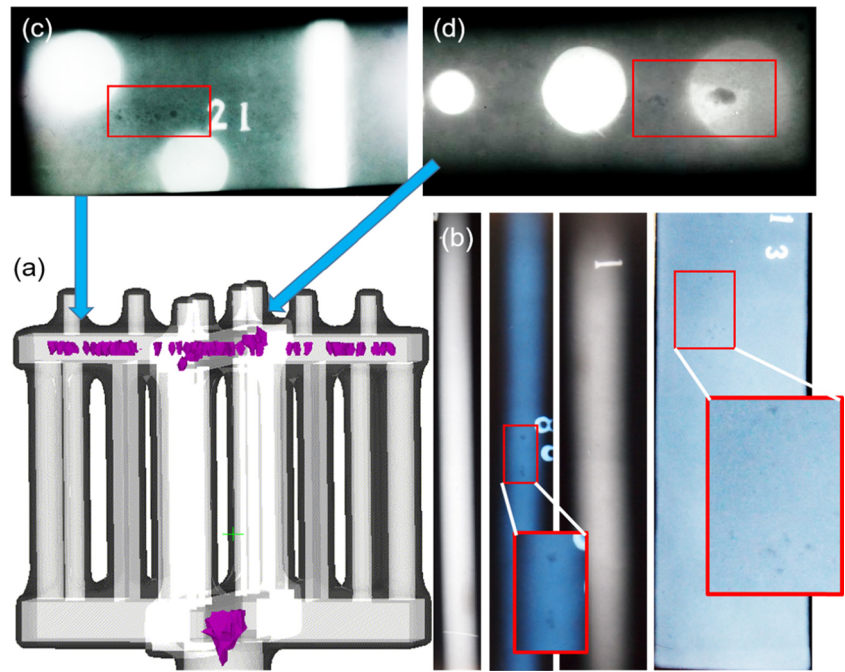
**Fig. 9** **a** Predicted shrinkage porosity via numerical simulation and the radiographs of the cast parts: **b** bars and sheet; **c** and **d** risers

### 3.1.3 Mold filling and defects

Counter-gravity casting was conducted with the casting parameters obtained in the simulation. Setting and actual pressure of bottom chamber in the casting process as a function of time is illustrated in Fig. 6. With the pressurization rate 9 kPa s$^{-1}$, the setting pressure reached 60 kPa in about 7 s. It can be observed that the actual pressure was lower than the setting pressure at initial stage of filling due to time delay. The pressure was held for more than 60 s to guarantee the solidification of cast part.

The obtained Ti-6Al-4V cast part in the counter-gravity casting process is shown in Fig. 7a. Cold shut was observed at the top of the 2-mm sheet, as shown in Fig. 7b, and was similar to the prediction of the simulation results. For the 2-mm sheet, the filling distance could reach up to 150 mm. By contrast, 180-mm sheets could be completely



**Fig. 10** Montage of typical micrographs of cross section from **a** 3-mm, **b** 6-mm, to **c** 9-mm wall thickness sheet; **d** Average grain size as functions of as-cast sheet thickness
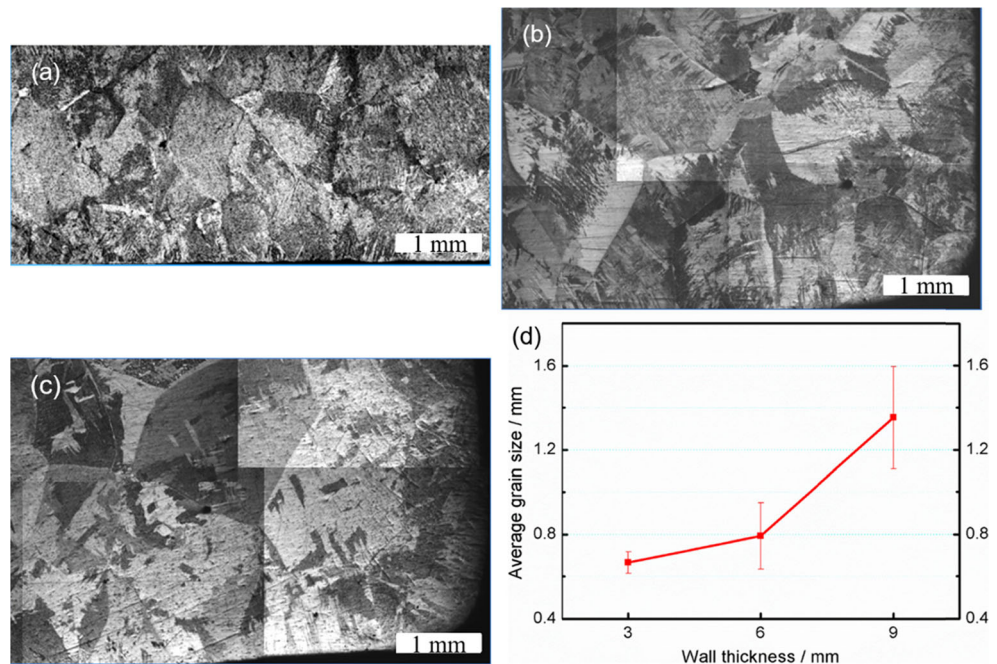
**Table 2** RT tensile properties of the Ti-6Al-4V alloy cast part with different diameters

| Dimensions (mm) | UTS (MPa) | YS (MPa) | Elongation (%) | Reduction in area (%) | $E$ (GPa) |
|---|---|---|---|---|---|
| Φ10 | 978.0±9.0 | 885.0±6.0 | 8.0±1.0 | 14.0±5.0 | 129.0±0.6 |
| Φ15 | 931.5±0.5 | 838.5±0.5 | 6.5±1.5 | 16.0±3.0 | 126.5±0.9 |
| Φ20 | 895.5±0.5 | 806.0±6.0 | 8.5±0.5 | 18.0±1.0 | 118.7±2.9 |

cast without any defects when the thickness was greater than 3 mm.

## 3.2 Solidification process

### 3.2.1 Temperature field in solidification

Convective and conductive heat exchanges were considered during the numerical simulation of casting. In investment casting, radiation was the dominant mode of heat transfer [17], especially in a vacuum environment because of the increased temperature of the mold relative to its surroundings. The contours of temperature in solidification was shown in Fig. 8. Inner and outer layers of the bars exhibited the different temperature profile, as marked in the black box in Fig. 8. The temperature of the outer part of the bar was lower than that of the inner part of the bar. This result could be ascribed to the self-radiation of the cast part.

### 3.2.2 Shrinkage porosity

Figure 9a presents the comparison of the numerical predictions and the experimental results of the shrinkage porosity. Shrinkage is mainly located at the runners and risers. The radiographs in Fig. 9b show that the bars and sheets were almost completely defect-free, except for several microporosities marked with red rectangles. However, some shrinkage porosities were observed at the centerline of the riser, as marked in Fig. 9c, d. Conclusion can be drawn that the predicted results are in good agreement with the experimental results.

## 3.3 Microstructure and tensile properties

Montage of typical micrographs of cross section from 3-, 6-, to 9-mm wall thickness sheet is shown in Fig. 10a–c. It is observed that equiaxed grains are formed regardless of the wall thickness. As demonstrated by Nastac et al. [4], one of the factors that influence the microstructure of titanium alloy cast is cooling rate. Average grain size of sheets with are statistically illustrated in Fig. 10d. Results show that the as-cast grain sizes increase with the thickness of sheets, i.e., decrease with the cooling rate.

Room temperature (RT) tensile tests were conducted on the cast part bars to evaluate the tensile properties of cast part produced via counter-gravity casting. Table 2 shows the mechanical properties of the Ti-6Al-4V alloy cast part with different dimensions. The results, including the average grain size, are illustrated as shown in Fig. 11. The average grain size of the bar also tends to increase with increasing diameter (Fig. 11a). As expected, the ultimate tensile strength (UTS), yield strength (YS), and elastic modulus decreased as dimension increased. However, the elongation and the area of reduction at fracture increased as dimension increased.

In ref. [18], the RT tensile properties of cast Ti-6Al-4V produced with gravity casting in HIP + annealing status (HIP at 899 °C and 103 MPa for 2 h plus annealed at 732 °C for 2 h) are as follows: UTS, 850 MPa; YS, 780 MPa; elongation, 8.6 %; reduction in area, 15.6 %. By comparison, the untreated as-cast in this work yielded higher strength and comparable ductility than the treated as-cast.



**Fig. 11** Grain size and room temperature tensile properties as functions of as-cast bar diameter: **a** Strength and average grain size and **b** ductility
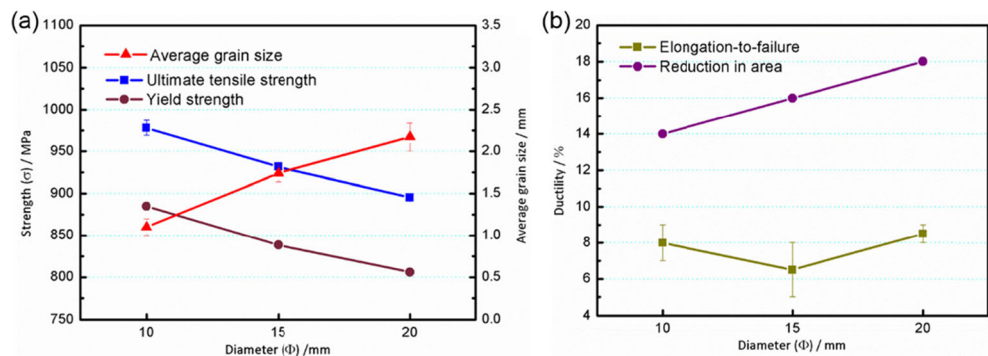
# 4 Conclusion

1. With the aid of numerical simulation, the optimized technology parameters were obtained. With pressure 60 kPa, and pressurization 9 kPa s$^{-1}$, sound Ti-6Al-4V cast part was produced via counter-gravity casting.

2. The filling capacity of counter-gravity casting is better than normal gravity casting, especially for thin-walled cast parts. The riser tube and the mold can be filled without any entrapment at a critical velocity of 0.5 m s$^{-1}$.

3. The minimum values of tensile properties are as below: UTS, 895 MPa; YS, 806 MPa; and elongation, 6.5 %. The results show that Ti-6Al-4V cast parts produced via counter-gravity casting exhibit good balance between strength and ductility, which are comparable to RT tensile properties of cast Ti-6Al-4V produced in gravity casting subjected to HIP + annealing status, i.e., UTS, 850 MPa; YS, 780 MPa; elongation, 8.6 %.

# References

1. Tang L, Du YT (2014) Experimental study on green electrical discharge machining in tap water of Ti-6Al-4V and parameters optimization. Int J Adv Manuf Technol 70(1–4):469–475
2. Jackson M, Dring K (2006) A review of advances in processing and metallurgy of titanium alloys. Mater Sci Technol 22:881–887
3. Pattnaik S, Karunakar DB, Jha PK (2012) Developments in investment casting process—a review. J Mater Process Technol 212:2332–2348
4. Nastac L, Gungor MN, Ucok I, Klug KL, Tack WT (2006) Advances in investment casting of Ti-6Al-4V alloy: a review. Int J Cast Met Res 19:73–93
5. Li CY, Wu SP, Guo JJ, Su YQ, Fu HZ (2008) Castability of thin walled titanium alloy castings in vertical centrifugal field. Mater Sci Technol 24:1209–1213
6. Shibata T (2007) Precision casting process for titanium alloy: LEVICAST. Titanium Japan 55:34–38
7. Xiong C, Ma YC, Chen B, Liu K, Li YY (2013) Modeling of filling and solidification process for TiAl exhaust valves during suction casting. Acta Metall Sin (China) 26:33–48
8. Fischer J, Stawarzcyk B, Trottmann A, Hämmerle CH (2009) Impact of thermal misfit on shear strength of veneering ceramic/zirconia composites. Dent Mater 25:419–423
9. Poirier DR, Poirier EJ (1992) Heat transfer fundamentals for metal casting. TMS, Pennsylvania
10. Niyama E, Uchida T, Morikawa M (1982) A method of shrinkage prediction and its application to steel casting practice. Int Cast Met J 7:52–63
11. Carlson KD, Beckermann C (2009) Prediction of shrinkage pore volume fraction using a dimensionless Niyama criterion. Metall Mater Trans A 40:163–175
12. Geiger GH, Poirier DR (1973) Transport phenomena in metallurgy. Addison-Wesley Publishing, New Jersey
13. Kuo JH, Hsu FL, Hwang WS (2001) Development of an interactive simulation system for the determination of the pressure–time relationship during the filling in a low pressure casting process. Sci Technol Adv Mater 2:131–145
14. Campbell J (2004) Castings practice: the ten rules of castings. Butterworth-Heinemann, Oxford
15. Itamura M, Adachi M, Murakami K, Harada T, Tamala M, Sato S, Maeda T (2002) Tensile properties of cast and mushy state rolled Al45Cu alloy and in situ Al45Cu5TiB2 composite. Int J Cast Met Res 15:173–178
16. Abdul-Karem W, Green N, Al-Raheem KF, Hasan AHA (2013) Effect of vibration after filling on mechanical reliability in thin wall investment casting with fillability filling regime-part 1. Int J Adv Manuf Technol 67:2075–2082
17. Tu JS, Foran RK, Hines AM, Aimone PR (1995) An integrated procedure for modeling investment castings. JOM 47:64–68
18. Donachie MJ (2000) Titanium: a technical guide. ASM International, Materials Park